A comprehensive study of ozone sensitivity with respect to emissions over Europe with a chemistry-transport model

Vivien Mallet and Bruno Sportisse

Cerea: Teaching and Research Center in Atmospheric Environment
Joint laboratory École Nationale des Ponts et Chaussées / Électricité de France R&D
http://www.enpc.fr/cerea/
Clime
Joint team Inria / École Nationale des Ponts et Chaussées
http://www-rocq.inria.fr/clime/

Abstract. A detailed sensitivity analysis of ozone concentrations with respect to anthropogenic and biogenic emissions is performed at European scale in summer 2001 through the use of the chemistry-transport model Polair3D. We estimate the time evolution of the sensitivities and the extent of the sensitive regions. We discriminate the chemical species to which photochemistry is the most sensitive. This work is intended as a preliminary study for inverse modeling of emissions. Local sensitivities are computed using a tangent linear model and an adjoint model of the underlying chemistry-transport model. Global sensitivities are approximated by means of Monte Carlo simulations. It is shown that NO emissions have a prominent impact and that VOC emissions also play an important role. Major emission sources are associated with the highest sensitivities, although a non-negligible sensitivity of the concentrations at observation stations can cover the whole domain. A typical relative sensitivity of ozone concentrations to NO emissions is about $6\mu g \cdot m^{-3}$, which is low as to compared to the error and the uncertainty in output concentrations.

1. Introduction

Emissions are a key input in air quality models and have therefore motivated many research efforts from the generation of emission data to their evaluation and improvement. In addition emission reductions are undertaken in order to satisfy the requirements of new laws and regulations in air pollution control. In this context the sensitivity of photochemical pollutants to their emitted precursors is of high interest. There are at least three motivations.

First the estimation of the sensitivities to emissions improves the understanding of the chemistry-transport models. It shows the prominent sensitivities and assesses the relative impact of emissions as compared to the known impacts of other processes. Second the sensitivities coupled with the uncertainty in the emissions provide an estimate of the uncertainty in the output concentrations due to the emissions. One may assess the reliability of a model and decide which part of the emissions should be improved as a priority. Third the sensitivity selects the emissions that could be optimized through inverse modeling [e.g., *Chang et al.*, 1997; *Mendoza-Dominguez and Russell*, 2001; *Elbern and Schmidt*, 2002; *Quélo*, 2004]. The aim is then to perform inverse modeling of the emissions to which the measured concentrations are sensitive enough to allow a valuable inversion. The conclusions of this paper are mainly related to the third option.

Inverse modeling of emissions should be performed on the most sensitive emission parameters. Otherwise the inversion would not be able to improve the model outputs (compared to measurements) or it would lead to unrealistic updates in the emissions. For instance the impact of the temporal distribution of emissions is weak [*Tao et al.*, 2004]. This study addresses in details the question of the prominent impacts. It notably ranks the emitted species, the emitting locations and the release time. It estimates the influence scope in space and time of the emissions. It also estimates the a priori quality of the observational network to perform inverse modeling.

There are several methods to estimate the sensitivities and they may be applied to different cases. In *Jiang et al.* [1997], the sensitivities are estimated along a single day and a single trajectory, and with finite differences. *Pryor* [1998] analyzes the impact on ozone concentrations of the emission changes over eight years. Using an adjoint model, *Menut* [2003] addresses, among other sensitivities, the sensitivity to emissions at regional scale, and *Schmidt and Martin* [2003] deal with European emissions and focus on their impact over Paris area.

This paper proposes a comprehensive study of the sensitivity to European emissions during summer 2001, using differentiated versions of a chemistry-transport model and a basic Monte Carlo method. The chemistry-transport model is differentiated into (1) a tangent linear model that produces the first-order derivatives of all outputs to a given model-input, and (2) an adjoint model that delivers the derivatives of a given model-output to all inputs (emissions, in this study). This way, the sensitivity is estimated with first-order derivatives. It is thus "local" and restricted to the given emission inventory. To obtain a more global picture of the sensitivity, Monte Carlo simulation are performed with perturbations in the emissions. The emissions are associated with log-normal probability density functions as advocated in *Hanna et al.* [1998, 2001]. Three sets of 200 simulations are generated to estimate the uncertainty due to NOx emissions, VOC emissions and biogenic emissions.

The paper is organized as follows. Section 2 describes the underlying modeling system, its physical components and its chemistry-transport model. The context is also detailed through the simulation of photochemistry, over Europe and during summer 2001, on which the sensitivity study is based. In section 3, we expose the sensitivities that are estimated and the techniques to compute them. The following sections report the results obtained with the tangent linear model (section 4), the adjoint model (section 5) and the Monte Carlo simulations (section 6).

0148-0227/05/$9.00

2. Modeling System

2.1. Description

The modeling system is Polyphemus (*Mallet et al.* [2005], available at `http://www.enpc.fr/cerea/polyphemus/`), version 0.2, notably based on the library for atmospheric chemistry and physics AtmoData [*Mallet and Sportisse*, 2005a] and the Eulerian chemistry-transport model Polair3D [*Boutahar et al.*, 2004].

Many configurations are available in Polyphemus. We have selected the most detailed physical parameterizations. The configuration is not chosen in order to provide the best forecasts but to use a reliable physics. This way the sensitivities will not be affected by artificial adjustments in the model.

The simulation is performed with the following physical parameterizations and input data:

1. meteorological data: the most accurate ECMWF data available for the period (i.e. $0.36^\circ \times 0.36^\circ$, the TL511 spectral resolution in the horizontal, 60 levels, time step of 3 hours, 12 hours forecast-cycles starting from analyzed fields);

2. land use coverage: USGS[1] finest land cover map (24 categories, 1km Lambert)

3. deposition velocities: the revised parameterization proposed in *Zhang et al.* [2003];

4. vertical diffusion: within the boundary layer, the Troen's and Mahrt's parameterization as described in *Troen and Mahrt* [1986], with the boundary-layer height provided by the ECMWF; above the boundary layer, the Louis' parameterization [*Louis*, 1979].

5. boundary conditions: daily means extracted from outputs of the global chemistry-transport model Mozart 2 [*Horowitz et al.*, 2003] run over a typical year.

Since the study deals with emissions, we provide more details about their generation. Anthropogenic emissions are generated with the EMEP[2] expert inventory for 2001. The spatial distribution comes along with the inventory. A typical time distribution of emissions, given for each month, day and hour [*GENEMIS*, 1994], is applied to each emission sector (called SNAP categories, i.e. sectors from the Selected Nomenclature for Air Pollution). The monthly coefficients also depend on the country, and the time zone of each country is taken into account in the hourly coefficients. As for the chemical distribution, the inventory species are disaggregated into real species using speciation coefficients provided in *Passant* [2002]. NOx emissions are split into 90% of NO (in mass), 9.2% of NO_2 and 0.8% of HONO. The aggregation into model species (for RACM) is done following *Middleton et al.* [1990].

Biogenic emissions are computed as advocated in *Simpson et al.* [1999]. Isoprene emissions are affected to the model species ISO (isoprene in RACM) and all emissions of terpenes are affected to API (α-pinene and other cyclic terpenes with one double bond in RACM).

Both anthropogenic and biogenic emissions are hourly emissions; the sensitivities are therefore computed with respect to hourly emissions.

As for numerical issues, the advection-diffusion-reaction equation is solved using:

1. a first-order operator splitting, the sequence being advection–diffusion–chemistry;

2. a direct space-time third-order advection scheme with a Koren flux-limiter advocated in *Verwer et al.* [1998];

3. a second-order order Rosenbrock method (suited for stiff problems) for diffusion and chemistry.

2.2. Test Case

The simulation takes place over Europe in the summer 2001. The domain is $[40.25^\circ N, 10.25^\circ W] \times [57.25^\circ N, 22.75^\circ E]$ (see figure 1), with $0.5^\circ \times 0.5^\circ$ cells, namely 33 cells along latitude and 65 cells along longitude. There are five cells along z whose centers are 25m, 325m, 900m, 1600m and 2500m. The top height of the last cell is 3000m, which is high enough to enclose the planetary boundary layer in most cases. The time step is 600s. The chemical mechanism is RACM (with 72 species and 237 reactions – see *Stockwell et al.* [1997]).

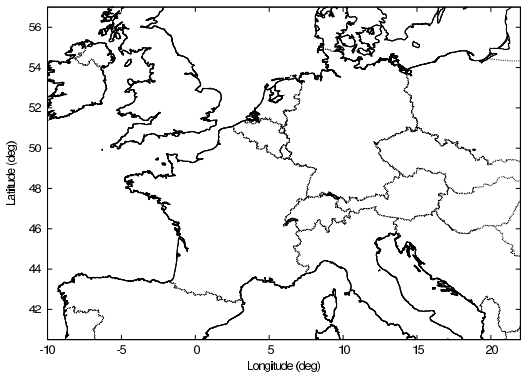

Figure 1. Domain $[40.25^\circ N, 10.25^\circ W] \times [57.25^\circ N, 22.75^\circ E]$ of the reference simulation.

Table 1. Statistics of the simulation for ozone concentrations over four months.

	EMEP network	Second network
	Hourly concentrations	
RMS	$26.0 \mu g \cdot m^{-3}$	$28.7 \mu g \cdot m^{-3}$
Correlation	57%	66%
Bias	$6.7 \mu g \cdot m^{-3}$	$12.6 \mu g \cdot m^{-3}$
	Concentrations at 1500 UT	
RMS	$21.7 \mu g \cdot m^{-3}$	$23.4 \mu g \cdot m^{-3}$
Correlation	61%	68%
Bias	$-3.7 \mu g \cdot m^{-3}$	$2.5 \mu g \cdot m^{-3}$

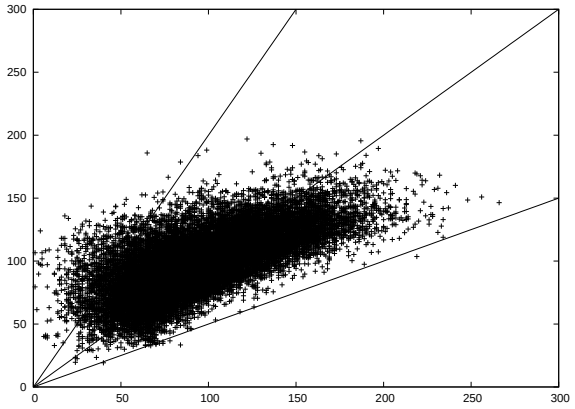

Figure 2. Scatter plot of simulated concentrations ($\mu g \cdot m^{-3}$) at 1500 UT versus measurements of the second network. Obviously, the model underestimates the highest concentrations. However the scatter plot confirms the satisfactory results summarized in table 1.

The simulation is evaluated with comparisons to measurements from two networks. The EMEP network for 2001 includes 151 stations that provide hourly measurements. The second set of stations provides up to 622,000 hourly measurements of ozone concentration from the 242 urban, periurban and rural stations over Europe that were used in the Pioneer experiment (`http://euler.lmd.polytechnique.fr/pioneer/`). Table 1 shows statistics about comparisons against hourly measurements and concentrations at 1500 UT (always close to the daily maximum for ozone).

Scatter plots (for the two networks) of concentrations at 1500 UT are shown in figure 2 and figure 3. Figures 4 and 5 show concentrations at 1500 UT at Montgeron (France) and at a station in the Netherlands. The root mean squares at these stations are $23.1\mu g \cdot m^{-3}$ and $23.3\mu g \cdot m^{-3}$ respectively, which is representative of the overall statistics for the second network.

According to these comparisons, the system gives satisfactory results in the chosen configuration and allows us to perform reliable sensitivity analyses.

3. Methodology

3.1. Sensitivities Selection

Among the sensitivities that may be computed, we study the sensitivities of ozone concentrations because:

1. ozone is always an important concern in air quality;

2. the modeling system performs well for ozone which is a long-range pollutant and for which the physical processes are well detailed;

3. the amount of measurements for ozone is much higher than for other species, which means that inverse modeling of emissions will mainly rely on assimilation of ozone measurements.

When it is necessary to further reduce the output parameters, we select ozone concentrations at network stations, to prepare inverse modeling of emissions. The focus is sometimes put on ozone peaks due to their usual importance.

The sensitivities may also be computed with respect to selected emissions. This limitation comes from computational costs. It is also justified because there are strongly emitting locations (cities) and the impact of changes in the emissions is assumed to be mainly due to these emissions. In the context of inverse modeling, it is natural to focus on the major emission sources due to their prominent impact.

In addition the output sensitivities may be aggregated. For instance, the sensitivities may be aggregated per emitted species so as to rank these species.

3.2. Estimated Sensitivities

We mainly compute relative sensitivities, as defined below. Let e be a scalar input (emission) of the model f and

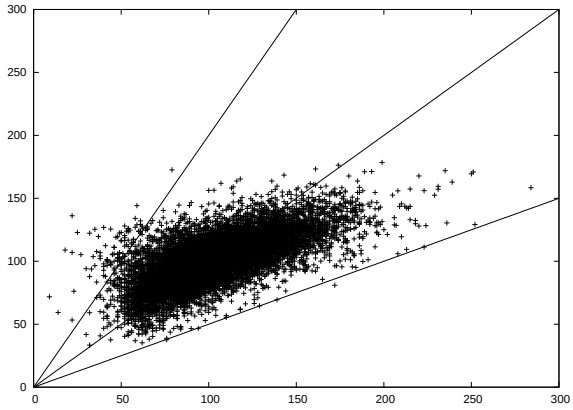

Figure 3. Scatter plot of simulated concentrations ($\mu g \cdot m^{-3}$) at 1500 UT versus measurements of the EMEP network. The same analysis as for the other network (figure 2) holds.

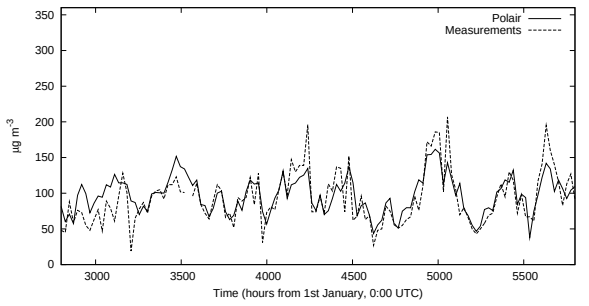

Figure 4. Concentrations at 1500 UT at Montgeron (France) from 27 April 2001 to 31 August 2001. The root mean square at this station is $23.1\mu g \cdot m^{-3}$.

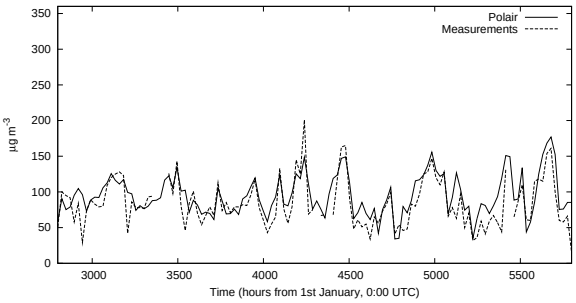

Figure 5. Concentrations at 1500 UT at a station in the Netherlands from 27 April 2001 to 31 August 2001. The root mean square at this station is $23.3\mu g \cdot m^{-3}$.

Table 2. Description of the sensitivities of $[O_3]_{h_c,i_c,j_c,k_c}$ with respect to E_{h_e,i_e,j_e} that are analyzed.

Variable	Possible values	Selected values	Comments
		Input emissions	
i_e	$[\![0,64]\!]$	–	Major sources
j_e	$[\![0,32]\!]$	–	Major sources
h_e	$[\![1,\infty[\![$	$[\![1,24]\!]$	Hourly emissions
		Output concentrations	
i_c	$[\![0,64]\!]$	$[\![0,64]\!]$	All cells
j_c	$[\![0,32]\!]$	$[\![0,32]\!]$	All cells
k_c	$[\![0,4]\!]$	$[\![0,1]\!]$	First two levels
h_c	$[\![0,\infty[\![$	$[\![h_e,h_e+24]\!]$	Hours from 16 July 2001 0000 UT or from 24 August 2001 0000 UT

c be a scalar output (ozone concentration):

$$c = f(e) \tag{1}$$

Since e is uncertain, we assume that it follows a Gaussian law: $e \sim \mathcal{N}(e_0, \sigma^2(e_0))$ where e_0 is the mean value of e and $\sigma(e_0)$ its standard deviation. We define the relative standard deviation as $\sigma^r(e_0) = \frac{\sigma(e_0)}{e_0}$.

We define the absolute sensitivity as:

$$s^a(e) = \frac{\partial f}{\partial e}(e) \tag{2}$$

and the relative sensitivity as:

$$s^r(e) = e\frac{\partial f}{\partial e}(e) \tag{3}$$

We estimate the sensitivity of the output c with respect to e using the linearized form of equation (1). Let:

$$\delta e := e - e_0 \sim \mathcal{N}\left(0, \sigma^2(e_0)\right) \tag{4}$$

From equation (1), $\delta c = \frac{\partial f}{\partial e}\delta e$ and

$$\delta c \sim \mathcal{N}\left(0, \left(\frac{\partial f}{\partial e}(e_0)\sigma(e_0)\right)^2\right) \tag{5}$$

This leads to:

$$c \sim \mathcal{N}\left(f(e_0), (s^r(e_0)\sigma^r(e_0))^2\right) \tag{6}$$

Assume that the most probable values for e are in $[e_0 - \sigma_0, e_0 + \sigma_0]$, then the most probable values of c are in $[f(e_0) - s^r\sigma_0^r, f(e_0) + s^r\sigma_0^r]$. Knowing that σ_0^r is usually given [*Hanna et al.*, 1998, 2001], the values that c may reach are determined by the relative sensitivity s^r. For instance, if the emission uncertainty is assumed to be equal to 30%, the output concentration c may be corrected by about $\pm 0.3 s^r$.

Moreover, according to *Hanna et al.* [1998, 2001], we can assume that all emissions have a similar relative standard deviation, with the exception of biogenic emissions. Therefore we directly compare relative sensitivities to identify the most sensitive emissions or emission parameters.

The extension to the vectorial case is straightforward and also shows that the relative sensitivity is a suitable criterion.

3.3. Evaluation Techniques

We use three techniques to estimate the sensitivities:

1. the tangent linear model (section 4): it is the differentiated version of the model and it returns the derivatives of all output concentrations with respect to a given emission (that is, for a given species, a given location and release time). The tangent linear model is well suited to evaluate the temporal and spatial impact of the major emitting locations.

2. the adjoint model (section 5): it provides the derivatives of a given output concentration with respect to all emissions. The adjoint model provides useful information with respect to the spatial extent of the sensitivity and the impact of all emissions at a given location.

3. Monte Carlo simulations (section 6): the emissions are perturbed according to a log-normal law (as suggested in *Hanna et al.* [1998, 2001]) to estimate the probability density function (PDF herein) of the output concentrations. This technique provides "global" sensitivities, not derivatives.

From the technical point of view, Monte Carlo simulations are handled by a dedicated module of Polyphemus. The tangent linear model and the adjoint model are obtained through automatic differentiation of Polair3D [*Mallet and Sportisse*, 2004].

4. Sensitivity Analysis with the Tangent Linear Model

4.1. Experiment Setup

Two periods are analyzed: the first one is 16–17 July 2001 and the second one is 24–25 August 2001. These periods were chosen due to good performances of the model. Moreover the second period is characterized by high ozone concentrations, which is a key situation to be investigated.

The sensitivity of ozone concentration $[\mathrm{O_3}]_{h_c,i_c,j_c,k_c}$ with respect to the emission E_{h_e,i_e,j_e} is:

$$\frac{\partial [\mathrm{O_3}]_{h_c,i_c,j_c,k_c}}{\partial E_{h_e,i_e,j_e}} \tag{7}$$

where the pollutant is emitted at the time step h_e, in the cell (i_e, j_e) and the concentration is taken at the time step h_c in the cell (i_c, j_c, z_c).

Table 2 shows values taken by h_c, i_c, j_c, z_c, h_e, i_e and j_e in this study with the tangent linear model.

For each species, a major emission source (i_e, j_e) is a source whose daily maximum flux is greater than or equal to the half of daily maximum flux (in the whole domain) for the species. The main sources were chosen because they should be associated with the highest relative sensitivities: if the absolute sensitivity slightly varies over the domain, the relative sensitivity will be much higher to the major sources. Moreover if emissions are selected for an inverse modeling experience over Europe, the emissions of the main cities will naturally be included. The number of cells considered as major emission sources is reported in table 3 for each species.

h_e is the emission time step. $h_e = 0$ at 0000 UT on 16 July 2001 (or 24 August 2001), and $h_e = 1$ at 0100 UT on 16 July 2001 (or 24 August 2001) since we deal with hourly emissions.

With the tangent linear model, the sensitivities of all output concentrations are available. One only selects the input emissions with respect to which the sensitivities are computed. However, because of storage constraints, there is still a selection in the output sensitivities. $i_c \in [\![0, 64]\!]$, $j_c \in [\![0, 32]\!]$ and $k_c \in [\![0, 1]\!]$ means that sensitivities in all cells of the first two levels are selected.

h_c represents hours from 16 July 2001 (or 24 August 2001) 0000 UT. For a given h_e, the sensitivity is non-zero only if $h_c \geq h_e$. It cannot be zero for $h_c = h_e$ because, as Polair3D solves the chemistry-transport equation between $h_e - 1$ and h_e, emissions are interpolated (linearly) between $h_e - 1$ and h_e. So the concentrations at time step h_e are sensitive to

Table 3. Number of sources per species with respect to which sensitivities are computed with the tangent linear model. The species are RACM emitted species and are defined precisely in *Stockwell et al.* [1997]. Note that isoprene (ISO) biogenic emissions are diffuse, which leads to a high number of cells.

Species	Number of cells	Species	Number of cells
ALD	7	ISO	36
API	10	KET	10
CO	7	NO	10
CSL	10	NO2	10
ETE	7	OLI	8
ETH	3	OLT	7
HC3	10	ORA2	6
HC5	9	SO2	11
HC8	12	TOL	10
HCHO	2	XYL	10
HONO	10		

emissions at time step h_e. The sensitivity is therefore returned from h_e and then for one day (i.e. until $h_e + 24$).

The number of major sources (sum over all species) is 205. Since there are 24 emission steps ($h_e \in [\![1, 24]\!]$), 4920 (one-day) simulations are performed.

This sensitivity study aims at determining to which parameters the model is sensitive. We want to rank the most important species, emission time steps, etc. To achieve this goal, maxima and norms of sensitivities are computed.

The analysis is mainly based on aggregated sensitivities. An aggregated sensitivity is a sum of sensitivities with a fixed input or output index and is computed through norms of vectors. For instance, let $S_{h_c}(h)$ be the vector of the sensitivities at the simulation time-step h ($h_c = h$), indexed by $(h_e, i_e, j_e, k_c, E, i_c, j_c)$:

$$S_{h_c}(h) = \left(\frac{1}{N_{\text{cells}}(E)} \frac{\partial \left[\text{O}_3\right]_{h_c=h,i_c,j_c,k_c}}{\partial E_{h_e,i_e,j_e}} \right)_{h_e,i_e,j_e,k_c,E,i_c,j_c} \quad (8)$$

where $N_{\text{cells}}(E)$ is the number of emission sources for species E with respect to which a sensitivity has been computed. $\frac{1}{N_{\text{cells}}(E)}$ is therefore a normalization factor needed to affect the same weight to all emitted species. From this vector, we compute two main indicators. $\max S_{h_c}(h)$ is useful to indicate whether emissions could have a strong local impact on concentrations at a given time step h. $\|S_{h_c}(h)\|_1$ denotes the norm one of the vector $S_{h_c}(h)$ and measures the global impact of emissions at the time step h.

These two indicators may be derived for all indices: S_{h_c}, S_{i_c}, S_{j_c}, S_{k_c}, S_E, S_{i_e}, S_{j_e} and S_{h_e}. Actually, i_c and j_c are put together: $S_{(i_c,j_c)}$; in the same way, we define $S_{(i_e,j_e)}$ and $S_{\Delta h=h_c-h_e}$.

Note that we have not provided the units (of the sensitivities) in the following results: the point is to compare the sensitivities. The impact on the concentrations is estimated in later sections (5 and 6).

Table 4. Maximum ozone sensitivity to the emitted species, i.e. $\max S_E$ for all species.

16 – 17 July		24 – 25 August	
Species	$\max S_E$	Species	$\max S_E$
NO	-6.2	NO	-7.9
ISO	$9.9{\cdot}10^{-1}$	ISO	$7.8{\cdot}10^{-1}$
HCHO	$4.0{\cdot}10^{-1}$	API	$3.9{\cdot}10^{-1}$
API	$3.0{\cdot}10^{-1}$	HCHO	$3.6{\cdot}10^{-1}$
NO2	$2.8{\cdot}10^{-1}$	NO2	$2.4{\cdot}10^{-1}$
OLI	$9.5{\cdot}10^{-2}$	OLI	$1.4{\cdot}10^{-1}$
OLT	$8.6{\cdot}10^{-2}$	HONO	$9.2{\cdot}10^{-2}$
XYL	$7.9{\cdot}10^{-2}$	OLT	$6.9{\cdot}10^{-2}$
HONO	$7.9{\cdot}10^{-2}$	XYL	$6.3{\cdot}10^{-2}$
SO2	$4.8{\cdot}10^{-2}$	SO2	$5.5{\cdot}10^{-2}$
ETE	$3.2{\cdot}10^{-2}$	CO	$2.8{\cdot}10^{-2}$
CO	$2.2{\cdot}10^{-2}$	ETE	$2.5{\cdot}10^{-2}$
HC3	$1.9{\cdot}10^{-2}$	HC3	$1.5{\cdot}10^{-2}$
TOL	$1.5{\cdot}10^{-2}$	HC8	$1.3{\cdot}10^{-2}$
HC5	$1.5{\cdot}10^{-2}$	TOL	$1.1{\cdot}10^{-2}$
HC8	$1.2{\cdot}10^{-2}$	HC5	$1.1{\cdot}10^{-2}$
KET	$3.8{\cdot}10^{-3}$	ALD	$3.6{\cdot}10^{-3}$
CSL	$-3.7{\cdot}10^{-3}$	KET	$2.9{\cdot}10^{-3}$
ALD	$2.9{\cdot}10^{-3}$	CSL	$-2.2{\cdot}10^{-3}$
ETH	$2.0{\cdot}10^{-4}$	ETH	$3.2{\cdot}10^{-4}$
ORA2	0.0	ORA2	0.0

Table 5. Ozone sensitivity to the emitted species (norm one), i.e. $\|S_E\|_1$ for all species.

16 – 17 July		24 – 25 August	
Species	$\|S_E\|_1$	Species	$\|S_E\|_1$
NO	$1.9{\cdot}10^{1}$	NO	$2.8{\cdot}10^{1}$
XYL	2.1	ISO	3.4
ISO	1.5	XYL	2.2
HCHO	$9.1{\cdot}10^{-1}$	HCHO	1.8
OLT	$8.4{\cdot}10^{-1}$	API	1.4
API	$6.9{\cdot}10^{-1}$	OLT	1.1
TOL	$6.3{\cdot}10^{-1}$	CO	1.0
ETE	$5.7{\cdot}10^{-1}$	NO2	$9.1{\cdot}10^{-1}$
NO2	$5.6{\cdot}10^{-1}$	ETE	$7.1{\cdot}10^{-1}$
CO	$5.4{\cdot}10^{-1}$	HC3	$6.7{\cdot}10^{-1}$
HC3	$5.2{\cdot}10^{-1}$	TOL	$6.4{\cdot}10^{-1}$
OLI	$3.2{\cdot}10^{-1}$	SO2	$5.7{\cdot}10^{-1}$
SO2	$3.1{\cdot}10^{-1}$	OLI	$4.4{\cdot}10^{-1}$
HC5	$2.7{\cdot}10^{-1}$	HC5	$4.0{\cdot}10^{-1}$
HC8	$2.4{\cdot}10^{-1}$	HC8	$2.7{\cdot}10^{-1}$
KET	$1.3{\cdot}10^{-1}$	HONO	$1.6{\cdot}10^{-1}$
HONO	$1.1{\cdot}10^{-1}$	KET	$1.1{\cdot}10^{-1}$
ALD	$5.0{\cdot}10^{-2}$	ALD	$9.8{\cdot}10^{-2}$
CSL	$2.6{\cdot}10^{-2}$	ETH	$2.3{\cdot}10^{-2}$
ETH	$1.1{\cdot}10^{-2}$	CSL	$1.9{\cdot}10^{-2}$
ORA2	0.0	ORA2	0.0

4.2. Results and Discussion

4.2.1. Sensitivity to Chemical Species: S_E

Tables 4 and 5 show the sensitivities (maxima and norm one respectively) with respect to all emitted species.

NO is clearly associated with the highest sensitivities as compared to the other species. The norm one identifies NO as the most important emitted species. The sensitivities with respect to NO_2 are about 30 times lower. There is a constant ratio between NO emissions and NO_2 emissions. According to the sensitivities, this ratio may be an important parameter because of the sensitivity to NO emissions. Nonetheless this ratio may have a slight impact if only NO_2 emissions are adjusted. In this context, inverse modeling of this ratio is hard to achieve.

There are highly reactive species such as CSL (cresol and other hydroxy substituted aromatics) that have only a slight influence on ozone concentrations. Actually they have a high absolute sensitivity (not reported here) but the relative sensitivity remains low because of their low emission fluxes. For instance, the maximum absolute sensitivity with respect to CSL is as high as the maximum sensitivity of ISO (isoprene) and its norm one is even significantly higher than ISO. It shows that the absolute sensitivities are not indicators suited in the perspective of inverse modeling.

The results raise the following question: what would be the sensitivity with respect to all volatile organic compounds as compared to NO? A rough idea may be drawn by summing up all the sensitivities. However a finer analysis is performed in this paper thanks to the use of the adjoint model (section 5).

Note that ozone concentrations are not sensitive to ORA2 emissions: ORA2 is only a product in RACM.

4.2.2. Temporal Sensitivity: $S_{\Delta h=h_c-h_e}$

It is of high interest to estimate the period over which emissions have some influence. Figure 6 shows the time evolution of the sensitivity.

The main effect is observed during the first hours. The maximum sensitivity quickly decreases, which tends to demonstrate that the emissions have only a local impact. Nevertheless the norm one of the sensitivity decreases slowly. The sensitivity after a few hours, is rather low but not negligible. As a conclusion, the emissions may have a strong local impact, and a more diffuse effect still lasts for several hours.

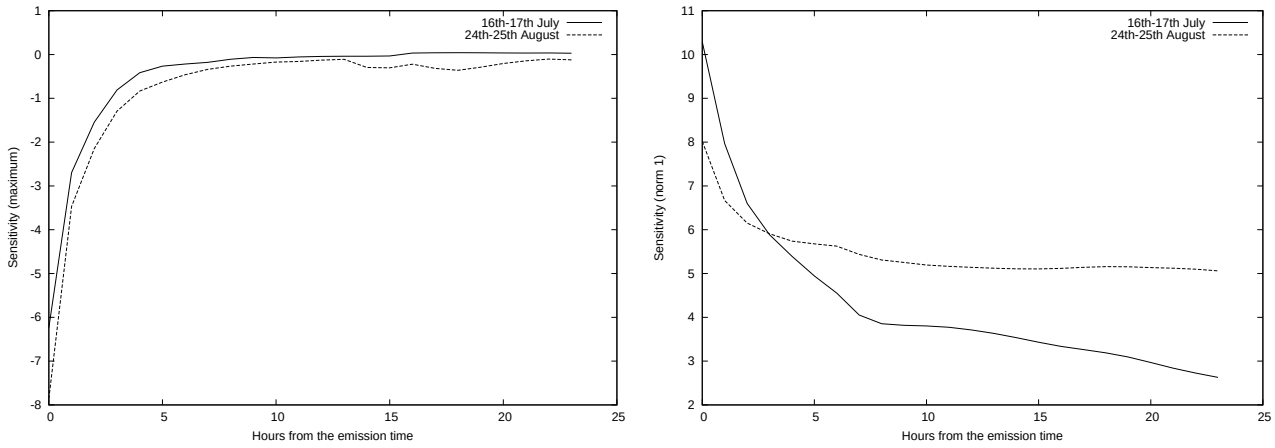

(a) (b)

Figure 6. Sensitivity (maximum on left, norm one on right) as function of the number of hours between the emission time and the simulated time. It shows the time evolution of the sensitivity.

4.2.3. Temporal Sensitivity: S_{h_c}

Depending on the hour in the day, ozone concentrations may be more or less sensitive to the emissions as shown in figure 8.

For each hour h_c, the norm one is computed with the available sensitivities, namely the sensitivities with respect to the emissions released within 24 hours before the hour h_c. But the number of emission times, before h_c and to which the sensitivities were computed, depends on h_c: if $h_c = 2$, only emissions released at $h_e = 1$ and $h_e = 2$ are taken into account; at the end, e.g. $h_c = 40$, the emissions taken into account are released at any $h_e \in [\![40 - 24, 24]\!]$ because the sensitivity to emissions released after $h_e = 24$ are not available (table 2). Hence the sensitivities shown in figure 8 should be carefully analyzed. However if the first hours and the last hours are discarded, the other sensitivities are reliable.

It appears that the concentrations at any time in the day may be influenced by the emissions.

4.2.4. Temporal Sensitivity: S_{h_e}

Figure 9 shows the sensitivities as function of the emission time. The point is to check whether all emissions in the day have a similar impact on the concentrations. Actually, since we analyze the relative sensitivities, its shows the possible impact of changes in the emissions within their uncertainty range, assumed to be the same relative range for every hour.

From the norm one, ozone concentrations seem to be more sensitive to the emissions in the daytime. However the sensitivity to the nightly emissions is not negligible as compared to the highest daytime sensitivity. The nightly emissions are strongly lower than the daytime emissions, but it appears that their absolute sensitivity is at least as high as for the daily emissions. This is probably due to the lower impact of the vertical diffusion during night.

4.2.5. Sensitivity to the Emission Location: $S_{(i_e,j_e)}$

There are 83 locations (i_e, j_e) (among the 205 (E, i_e, j_e) combinations – see table 3). It is not possible to point out clearly which locations lead to the highest sensitivities because (1) the sensitivity depends on the emitted pollutant, and (2) there is no gap in the list of sensitivities. The locations have been sorted from the most sensitive location to the less sensitive one. For the experiment over 16–17 July, the fifteen first sensitivities (norm 1) are: 8.90, 5.92, 5.81, 5.75, 5.13, 4.00, 3.91, 3.89, 3.01, 2.69, 2.69, 2.42, 2.30, 2.25, 1.86. It then decreases slowly down to 0.07 (if the sensitivities to ORA2 are excluded). The 37th location is associated with a sensitivity lower than a tenth of the sensitivity associated with the first location (8.90).

The highest sensitivities are mainly reached at the locations where NO is emitted. It seems more relevant to rank the locations for each species, i.e. to analyze S_{E,i_e,j_e} instead of S_{i_e,j_e}. Then there are too few locations per species to draw reliable conclusions. Nevertheless, for each species, it appears that the sensitivities rapidly decrease among the locations. For most species, associated with about ten cells (see the table 3), there is a ratio of about three between the first sensitivity and the last one. Recall that the emission locations were included in the experiment if their emission flux was greater than the half of the highest emission flux. Therefore, if the absolute sensitivities were constant, the ratio between the extreme sensitivities would be two. The actual decrease is higher, which tends to show that ozone concentrations are mainly sensitive to a few emission locations.

4.2.6. Sensitivity to the Concentration Location: $S_{(i_c,j_c)}$

There are 2145 cells that may be sorted in the same way as for the emission locations. The sensitivities also decrease

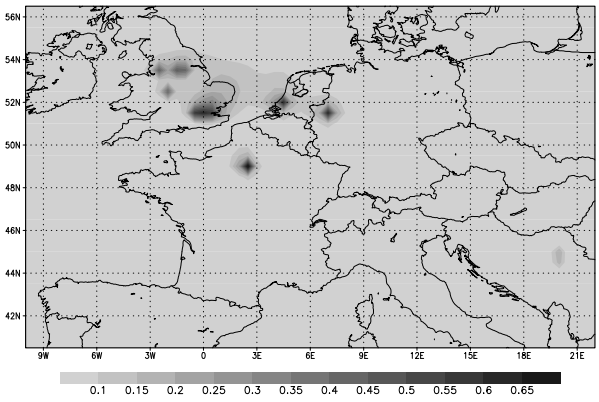

Figure 7. Relative sensitivities $S_{(i_c,j_c)}$ of output concentrations (mean over 16–17 July and 24–25 August). The highest sensitivities are mainly reached in the vicinity of the major emission sources.

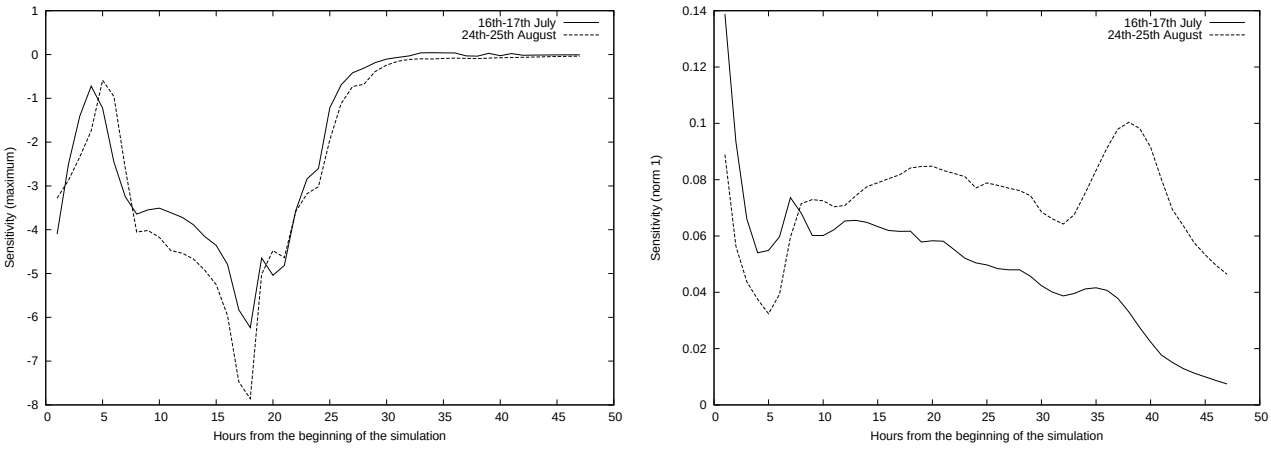

(a) (b)

Figure 8. Sensitivity (maximum on left, norm one on right) as function of the hour h_c in the day.

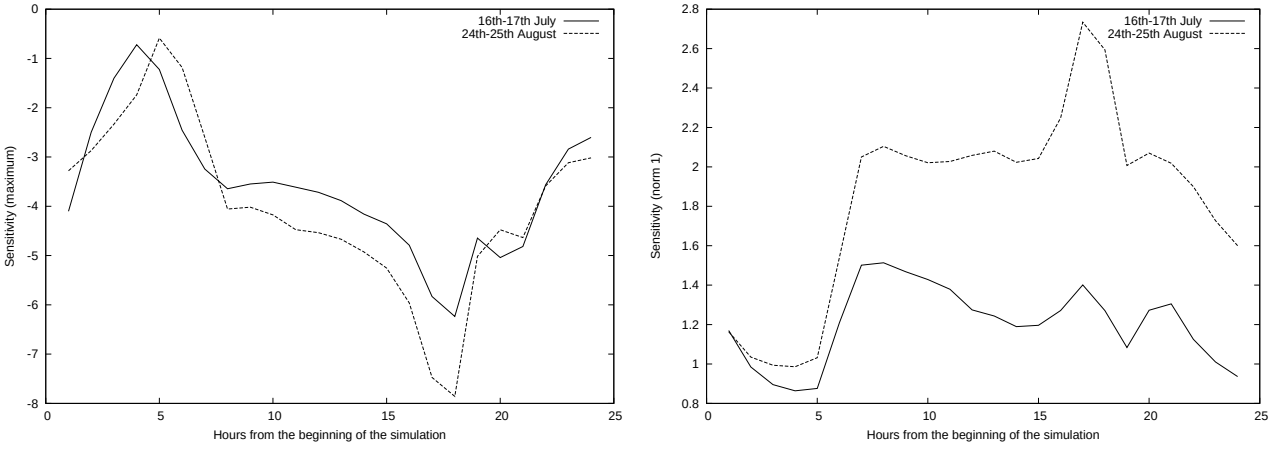

(c) (d)

Figure 9. Sensitivity (maximum on left, norm one on right) as function of the emission time.

slowly. Again, the cells where NO is strongly emitted (i.e. the 10 cells $(i_{\mathrm{NO}}, j_{\mathrm{NO}})$) lead to high sensitivities in their neighborhood. The 88th cell is associated with a sensitivity lower than a tenth of the highest sensitivity (norm one). Since there are 85 emitting points to which the sensitivity was computed, it means that highest sensitivities are mostly found close to the main sources. This is illustrated by figure 7.

4.2.7. Vertical Profile

As previously mentioned, sensitivities are available only in the first two vertical levels. The maximum of S_{k_c} is found in the first level (twice as high as the maximum in the second level), but the norm one is similar in both levels.

4.3. Validity of the Study

There are mainly two limitations that may question the validity of the study: (1) the amount of emission points with respect to which the sensitivities are computed, (2) the number of experiments (two periods).

As for the number of emission points, there is no indication, in the previous analyses, that the inclusion of more sources would change the results: the highest relative sensitivities are chiefly due to the highest emission locations. However this experiment with the tangent linear model only claims a validity with respect to the strongest emission sources. In section 5, the sensitivities are computed with respect to all locations.

There are only two experiments: one in July and another in August. Both give similar results even if the meteorological conditions and the ozone concentrations are strongly different. Moreover the same experiment has also been performed over 11–12 July 2001, but with an older version of the simulation system. The results are not reported in this paper because the simulation relied on less satisfactory parameterizations (Wesely's parameterization for deposition velocities – *Wesely* [1989] –, Louis' closure – *Louis* [1979] – for the vertical diffusion, a rough cloud attenuation scheme) and, for instance, its RMS at 1500 UT was about $25\mu\mathrm{g}\cdot\mathrm{m}^{-3}$. Nevertheless, this experiment led to the same conclusions as the two experiments detailed in this paper. It means that the results are repeatable, even with other models. Finally, a less detailed analysis, but still computing relative sensitivities with the tangent linear model of Polair3D, has been performed at regional scale over Île-de-France. As far as the

results may be compared, the conclusions of the regional study are consistent with the analyses at continental scale.

5. Sensitivity Analysis with the Adjoint Model

5.1. Experiment Setup

The sensitivities are computed over the same periods, starting from 16 July 2001 and 24 August 2001. While the tangent linear model requires the choice of a limited set of emissions, applying the adjoint model once provides the sensitivities of a scalar value (i.e. the ozone concentration in a given cell and at a given time) with respect to all emissions. In this study, the sensitivities are computed at all cells that contain an EMEP station. There are 105 such stations in 103 cells. The sensitivity of ozone concentrations at 1500 UT are selected because they are close to the peaks which are a major concern in ozone forecasts. The 206 simulation (103 cells, 2 periods) are performed over 3 days and a half: starting 16 July 2001 and 24 August 2001 at 0000 UT and ending 19 July and 27 August at 1500 UT.

In addition, the time evolution is analyzed at two stations of different nature: one that contains Paris (highly emitting area) and another one containing the EMEP station Montandon. Note that EMEP stations are not located in strongly emitting regions, in order to measure the long-range transboundary pollution.

The sensitivities are not computed with respect to all model emissions but with respect to inventory emissions. Inventory emissions are provided on the EMEP grid (polar-stereographic projection) and are gathered into four inventory species: NOx, NMVOC (volatile organic compounds), SOx and CO (we focus on NOx and NMVOC in this study, due to their prominent impact). The sensitivities are computed with respect to yearly emissions which are the raw data provided by EMEP. Actually the gradients are the derivatives with respect to EMEP yearly emissions but over the period of the simulation. It means that the contributions (to the gradient) coming from emissions released before the beginning of the simulation are discarded. However these discarded contributions are negligible.

5.2. Results and Discussion

5.2.1. Distribution over the EMEP Network

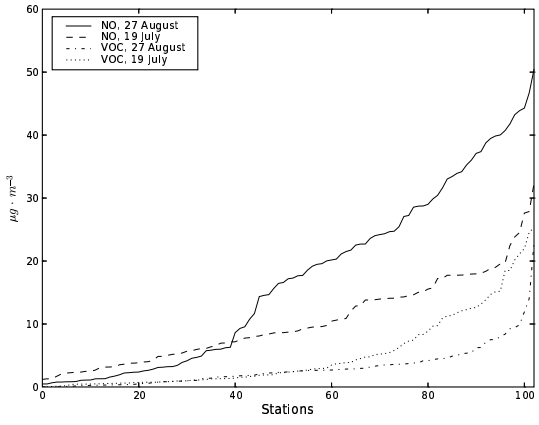

Figure 10. Norm one of the relative sensitivity for all stations. The sensitivities of the four cases are sorted independently so that they are increasing functions of the stations. The stations order is not the same one in the four cases.

For each station, we compute the norm one of the sensitivity: the sum over all cells of the relative sensitivities. It estimates the impact that changes in the emissions can have at the stations. The distribution of the norm one over the stations is shown in figure 10. The means over all stations is $17.2\mu g \cdot m^{-3}$ and $10.3\mu g \cdot m^{-3}$ for NO emissions (27 August and 19 July respectively), $3.0\mu g \cdot m^{-3}$ and $5.1\mu g \cdot m^{-3}$ for NMVOC emissions (27 August and 19 July respectively).

The sensitivity to NO emissions is at least twice as high as the sensitivity to NMVOC emissions, which is also the ratio that may be computed from table 5. With this ratio, inverse modeling of emissions may be performed with both NO and NMVOC emissions as control parameters.

The sensitivities are highly spread among the stations, from stations at which ozone concentrations are not sensitive to emissions to stations with high sensitivities (up to $50.4\mu g \cdot m^{-3}$). The correlation between the sensitivities for 19 July and 27 August is low (about 15%): the sensitivities strongly vary due to the conditions. However if one considers at each station the average of the sensitivities for the two periods, there are still several stations with a low sensitivity. The sensitivities in other meteorological conditions would be useful to confirm this remark.

5.2.2. Spatial Extent

For inverse modeling, it is useful to check that the observations are sensitive to emissions of the whole domain. Otherwise measurements would not bring enough information to invert all emissions. The spatial extent of the sensitivities depends on:

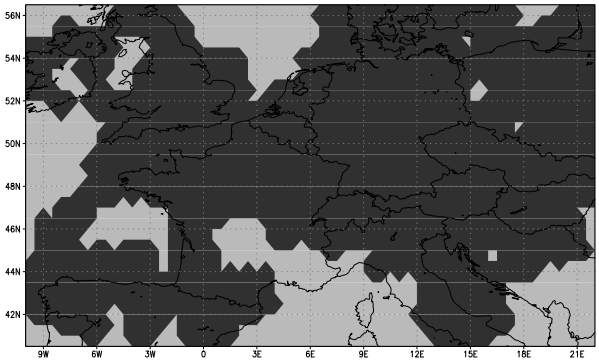

Figure 11. Area covered by the significant sensitivities associated with all stations of the EMEP network, for NO emissions and for 19 July.

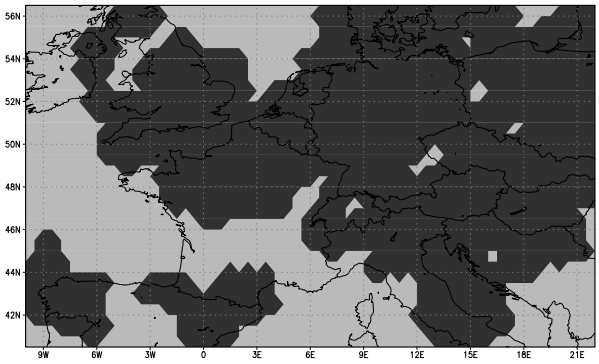

Figure 12. Area covered by the significant sensitivities associated with selected stations of the EMEP network, for NO emissions and for 19 July. 75% of EMEP stations are included due to their high sensitivity. This figure can be compared with figure 11 in which all EMEP stations are included.

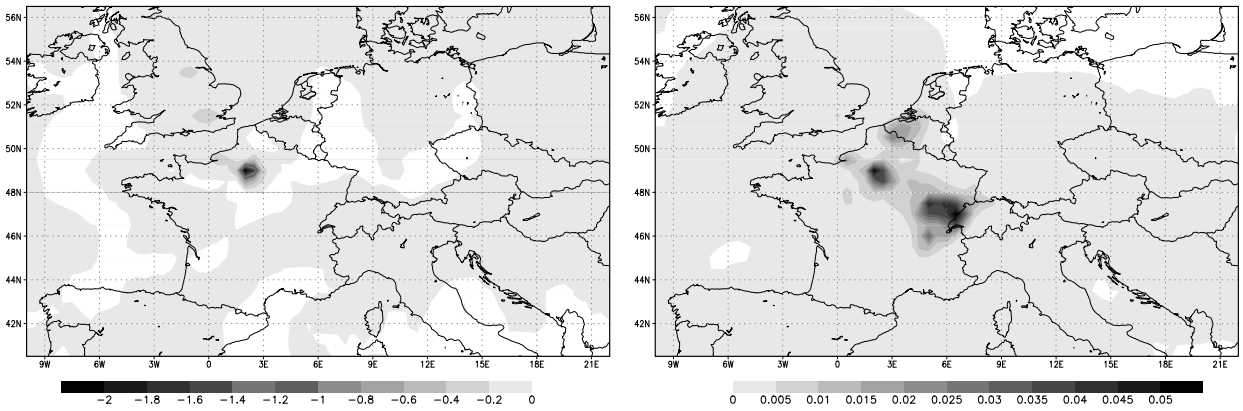

(a) (b)

Figure 13. Sensitivity (in $\mu g \cdot m^{-3}$) of ozone concentrations at 1500UT (ozone peak) on 26 August 2001. On the left, the figure shows the sensitivity of the ozone concentration at Paris with respect to NOx emissions. On the right, the figure shows the sensitivity of the ozone concentration at the EMEP station Montandon with respect to NMVOC emissions. The extent of the sensitivity may strongly differ depending on the station and the emitted pollutants.

1. the meteorological conditions (notably wind velocities);

2. the species (chemical reactivity): because of the efficient titration of ozone by NO, the sensitivity to NOx emissions tend to be more local than the sensitivity to NMVOC;

3. the emission locations (the relative sensitivities tend to be high at emission locations): the sensitivities usually have a larger extent when they are computed at stations far from the major emission sources.

It appears that the spatial extent may strongly differ due to these factors. For instance, in figure 13, a local sensitivity is obtained over Paris to NOx emissions and a larger extent is found for the sensitivity of a concentration at Montandon to NMVOC emissions.

To assess the impact of all stations, we first associate a spatial extent to each station. For each station, we select all emission cells to which the ozone concentration (at 1500 UT) has a significant sensitivity. A sensitivity is assumed to be significant if it is among the highest sensitivities whose sum contributes to 75% of the overall sensitivity (norm one). It is found that the domain is well covered, as shown in figure 11 (example with NO emissions and for 19 July). However it includes the spatial extent of stations with low sensitivities. Figure 11 reports the area covered in case where 25% of the stations are discarded because of their low sensitivities (less than $5\mu g \cdot m^{-3}$ – see figure 10). The area covers the main part of the domain. The same is observed for 24 August. As for VOC emissions, the area is even bigger. Providing that the sensitivities are high enough, this is a promising result for inverse modeling.

5.2.3. Time Evolution

The sensitivities are computed using the adjoint model which integrates the chemistry-transport equation backward in time. In the previous sections, the integration was performed over three days and a half: it was assumed that emissions released before have a negligible impact. The evolution of the computed sensitivities backward in time shows

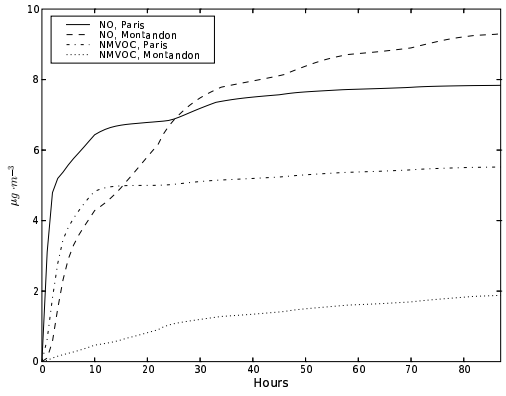

Figure 14. Norm one of cumulated relative sensitivities as function of the number of hours over which the backward integration is performed.

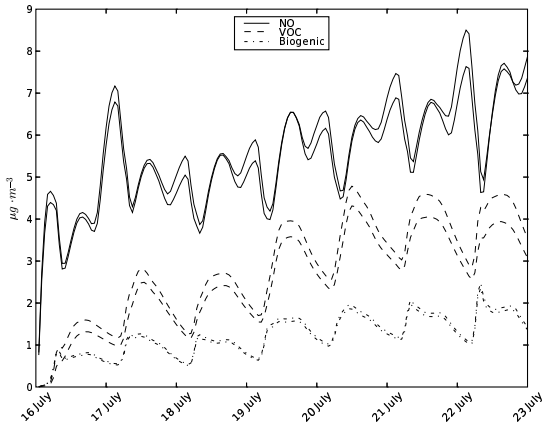

Figure 15. Time evolution of the standard deviation (averaged over the whole domain) of the ensemble for first-layer ozone concentrations. It is shown for NO, VOC and biogenic emissions for the full ensemble (200 simulations) and for restricted ensemble (100 simulations).

to which hourly emissions the ozone concentrations are sensitive. As shown in figure 14, ozone concentrations (still at 1500 UT) are mainly sensitive to the emission released in the first hours. This is especially true over Paris due to the high local emissions which constitute the main part of the (relative) sensitivity.

6. Sensitivity Analysis with Monte Carlo Simulations

As previously mentioned, the Monte Carlo simulations are performed in order to estimate "global" sensitivities. Moreover the emissions in the whole domain are perturbed, which provides additional information to the sensitivities to the major emission sources (section 4) or to the sensitivities over the EMEP network (section 5).

6.1. Experiment Setup

The Monte Carlo simulations are performed over one week: from 16 July 2001 to 22 July 2001 (included). The initial conditions are the same ones for all simulations. Three sets of two hundred simulations are performed with perturbations in NO emissions (first set), VOC emissions without biogenic emissions (second set) and biogenic emissions (third set). For each simulation the whole emission field is modified, that is, the emissions at all time steps and in all cells. Note that, for a perturbation in VOC emissions, all VOC species are perturbed with the same coefficient. This is also true for biogenic emissions (actually ISO and API).

From *Hanna et al.* [2001], we assume that emissions (including biogenic emissions) have a log-normal distribution with standard deviation of the log-transformed data set to 0.203. It roughly means that the emissions mainly vary within $\pm 50\%$ of the reference value. This is the uncertainty proposed in *Hanna et al.* [2001] for major emission points. Other emissions, notably biogenic emissions, are associated with higher uncertainty in *Hanna et al.* [2001]. However the point of this paper is to estimate the sensitivity, not the uncertainty. All emissions are therefore perturbed in the same way.

6.2. Results and Discussion

6.2.1. Sensitivity to Inventory Species

The sensitivity is estimated with the standard deviation in an ensemble for output ozone concentrations. In figure 15, the averages over the whole domain of standard deviation of the ensembles (for ozone concentrations in the first layer) are shown for NO, VOC and biogenic emissions. The same results for a restricted set of 100 simulations are also reported to demonstrate that the ensemble has reasonably converged.

In figure 15, it appears that the emissions have an impact in a very few hours, especially NO emissions. Then the impact slowly increases due to accumulation in the domain for about four days. The sensitivity is stabilized in the last three days.

NO emissions still imply the highest sensitivity with an average standard deviation of $6.3\mu g \cdot m^{-3}$ for the last three days, to be compared with $3.9\mu g \cdot m^{-3}$ for VOC emissions and $1.5\mu g \cdot m^{-3}$ for biogenic emissions. The sensitivity to VOC and biogenic emissions is close to the sensitivity to NO emissions. A consequence for inverse modeling of emissions is that VOC and NO emissions should be both optimized.

6.2.2. Sensitivity Spatial-Distribution

The spatial distribution of the sensitivity is estimated with the distribution of the standard deviation of the ensemble. The sensitivity due to NO emissions is more spread than the sensitivity to VOC emissions. Nevertheless it appears that there is a noticeable dependence on the meteorological conditions. The sensitivity is high in the regions that are in the plume of the major emission locations, especially of emissions from Great Britain. Otherwise the distribution of the sensitivity strongly varies from one day to another. Simulations over a longer period should be performed to draw further conclusions.

6.2.3. "Global" Sensitivity

The probability density function of the concentrations shows how the system is sensitive to the most probable emissions. In figures 16 and 17, the distributions of the minima and the maxima of ozone concentrations are shown for changes in NO emissions and changes in VOC emissions, which provides more details than the averaged standard deviations of section 6.2.1. The distributions roughly show the characteristics of a log-normal distribution. They would be log-normal distributions in case the model is linear since the emissions are assumed to be log-normal. The shape of the distribution (maximum probability on left or on right) is due to the sign of the sensitivity: additional NO emissions titrate ozone concentrations whereas additional VOC emissions lead to ozone production. Another remark is the high sensitivities of daily minima to NO emissions.

In figures 16 and 17, the analyzed concentrations are mean concentrations that may hide compensations: the emissions could increase ozone production in a given region (or at given hours in the day) while it could decrease ozone production somewhere else. To check that there is a clear tendency in the whole domain, the proportion of concentrations (in each cell and each hour in the last three days) above the reference concentrations (that is, concentrations of the simulation without perturbations in the emissions) is shown in figure 18. Changes in VOC emissions lead to either lower or higher ozone daily maxima in all cells. NO emissions are not associated with such a clear dependency but there are still two distinct modes in the distribution. The same behaviors for VOC and NO emissions are found for the daily minima. Moreover the biogenic emissions show the same behavior as the other VOC emissions.

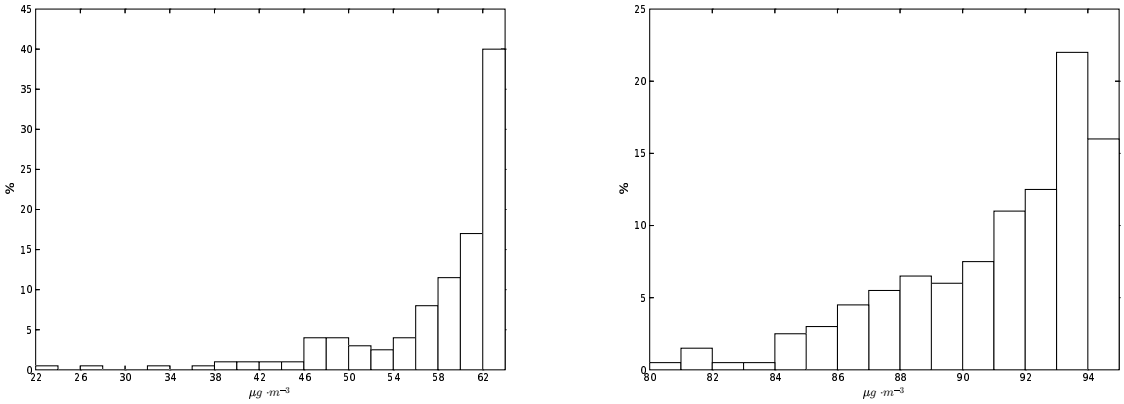

(a) (b)

Figure 16. Distributions of the means of the daily ozone minima (left) and maxima (right) due to changes in NO emissions. The means are computed over the last three days of the simulation (20–22 July) and over the whole domain from which a band of three cells has been discarded (to minimize the influence of the boundary conditions). The reference simulation is associated with a minimum of $62.7\mu g \cdot m^{-3}$ and a maximum of $92.3\mu g \cdot m^{-3}$.

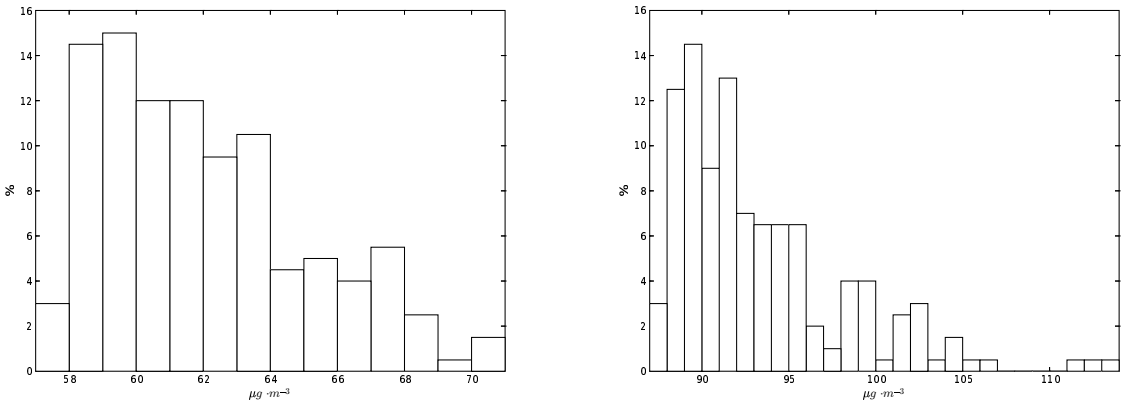

(c) (d)

Figure 17. Same distributions as in figure 16, but due to changes in VOC emissions.

7. Conclusion

From the previous results, it appears that ozone concentrations are more sensitive to NO emissions than to emissions of any other species. However the sensitivity to all VOC species is not negligible as compared to the sensitivity to NO emissions. The ratio between the sensitivities to NO emissions and to VOC emissions is about two in the studied cases and depends on the meteorological conditions and on the involved locations. Inverse modeling of emissions would therefore be performed on both NO and VOC emissions.

A possible impact of NO emissions is estimated with a relative sensitivity of $6.3\mu g \cdot m^{-3}$, which is rather low knowing that the uncertainty in the emissions is about $\pm 50\%$ and that the error on ozone concentrations (root mean square) is about $20\mu g \cdot m^{-3}$. It should also be compared to the uncertainty due to the physical parameterizations and numerical approximations, e.g. at least $10\mu g \cdot m^{-3}$ on ozone peaks [*Mallet and Sportisse*, 2005b]. It means that inverse modeling of emissions is a difficult task and that results from such an experiment should be carefully checked. The investigation of second-order sensitivities should be performed (see *Quélo et al.* [2005] for an application at regional scale).

On the other hand, the emissions have a rather local effect in time and space, and the sensitivities can be high close to strongly emitting locations. Inverse modeling of these sources could benefit from these high sensitivities. Moreover concentrations at every hours are sensitive to emissions, and, in the same way, emissions released at any time can be associated with high sensitivities. Depending on the abilities to forecast all concentrations, inverse modeling may take advantage of all observations and may retrieve emissions released at any time. We also found that the spatial

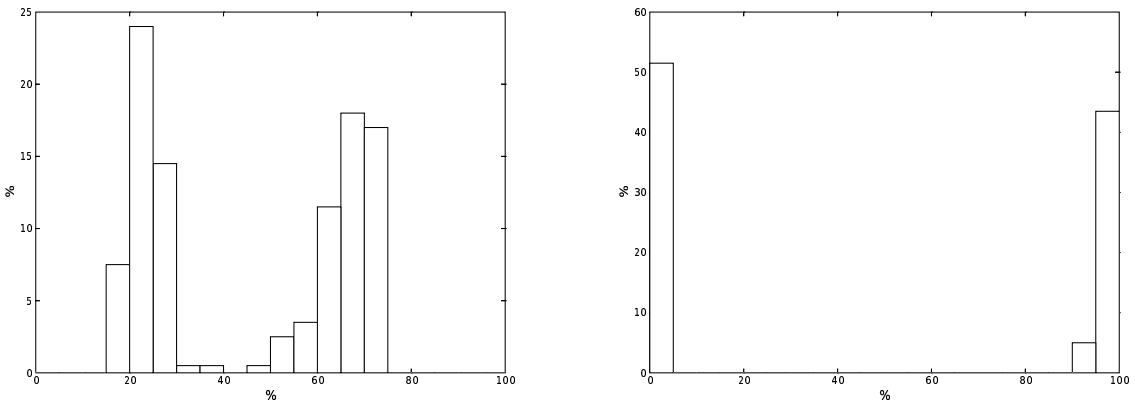

(a) (b)

Figure 18. Percentage of simulations versus the percentage of ozone daily maxima (in all cells in the domain minus a three-cell band at the borders) above the reference concentrations for NO emissions (left) and for VOC emissions (right). Bars whose abscissae are below 50% are associated with simulations in which most peaks are below the reference peaks.

distribution of the sensitivities covers the whole simulation domain.

Acknowledgments. The first author is partially supported by the Île-de-France region. We thank Denis Quélo (Cerea) for his work on the differentiated versions of Polair3D and for his involvement through a sensitivity study with the tangent linear model at regional scale. We thank Mohamed Aissaoui whose tool allowed us to perform Monte Carlo simulations. We are grateful to Cécile Honoré (Ineris) for her help with the emission generation. Genemis (through Ademe) provided the temporal factors. Finally we thank Robert Vautard (IPSL) and the monitoring networks (notably EMEP) for ozone observations.

Notes

1. U.S. Geological Survey.
2. Co-operative Programme for Monitoring and Evaluation of the Long-range Transmission of Air Pollutants in Europe.

References

Boutahar, J., S. Lacour, V. Mallet, D. Quélo, Y. Roustan, and B. Sportisse, Development and validation of a fully modular platform for numerical modelling of air pollution: POLAIR, *Int. J. Environment and Pollution*, *22*(1/2), 17–28, 2004.

Chang, M. E., D. E. Hartley, C. Cardelino, D. Haas-Laursen, and W.-L. Chang, On using inverse methods for resolving emissions with large spatial inhomogeneities, *J. Geophys. Res.*, *102*(D13), 16,023–16,036, 1997.

Elbern, H., and H. Schmidt, 4D-var data assimilation and its numerical implications for case study analyses, in *Atmospheric Modeling*, edited by D. P. Chock and G. R. Carmichael, pp. 165–183, IMA, Springer, 2002.

GENEMIS, Genemis (generation and evaluation of emission data) annual report 1993, *Tech. rep.*, EUROTRAC, 1994.

Hanna, S. R., J. C. Chang, and M. E. Fernau, Monte Carlo estimates of uncertainties in predictions by a photochemical grid model (UAM-IV) due to uncertainties in input variables, *Atmos. Env.*, *32*(21), 3,619–3,628, 1998.

Hanna, S. R., Z. Lu, H. C. Frey, N. Wheeler, J. Vukovich, S. Arunachalam, M. Fernau, and D. A. Hansen, Uncertainties in predicted ozone concentrations due to input uncertainties for the UAM-V photochemical grid model applied to the July 1995 OTAG domain, *Atmos. Env.*, *35*(5), 891–903, 2001.

Horowitz, L. W., et al., A global simulation of tropospheric ozone and related tracers: description and evaluation of MOZART, version 2, *J. Geophys. Res.*, *108*(D24), 2003.

Jiang, W., D. L. Singleton, M. Hedley, and R. McLaren, Sensitivity of ozone concentrations to VOC and NO_x emissions in the Canadian Lower Fraser Valley, *Atmos. Env.*, *31*(4), 627–638, 1997.

Louis, J.-F., A parametric model of vertical eddy fluxes in the atmosphere, *Boundary-Layer Meteorology*, *17*, 187–202, 1979.

Mallet, V., and B. Sportisse, 3-D chemistry-transport model Polair: numerical issues, validation and automatic-differentiation strategy, *Atmos. Chem. Phys. Discuss.*, *4*, 1,371–1,392, 2004.

Mallet, V., and B. Sportisse, Data processing and parameterizations in atmospheric chemistry and physics: the AtmoData library, *Submitted to Atmospheric Environment*, 2005a.

Mallet, V., and B. Sportisse, Uncertainty in chemistry-transport models due to physical parameterizations and numerical approximations: an ensemble approach, *Submitted to J. Geophys. Res.*, 2005b.

Mallet, V., D. Quélo, and B. Sportisse, Software architecture of an ideal modeling platform in air quality – A first step: Polyphemus, *Submitted to Atmospheric Environment*, 2005.

Mendoza-Dominguez, A., and A. G. Russell, Estimation of emission adjustments from the application of four-dimensional data assimilation to photochemical air quality modeling, *Atmos. Env.*, *35*, 2,879–2,894, 2001.

Menut, L., Adjoint modeling for atmospheric pollution process sensitivity at regional scale, *J. Geophys. Res.*, *108*(D17), 8,562, 2003.

Middleton, P., W. R. Stockwell, and W. P. L. Carter, Aggregation and analysis of volatile organic compound emissions for regional modeling, *Atmos. Env.*, *24A*(5), 1,107–1,133, 1990.

Passant, N. R., Speciation of UK emissions of NMVOC, *Tech. Rep. AEAT/ENV/0545*, AEA Technology, 2002.

Pryor, S. C., A case study of emission changes and ozone responses, *Atmos. Env.*, *32*(2), 123–131, 1998.

Quélo, D., Simulation numérique et assimilation de données variationnelle pour la dispersion atmosphérique de polluants, Ph.D. thesis, École Nationale des Ponts et Chaussées, 2004.

Quélo, D., V. Mallet, and B. Sportisse, Inverse modeling of NO_x emissions at regional scale over Northern France. Preliminary investigation of the second-order sensitivity, *Submitted to J. Geophys. Res.*, 2005.

Schmidt, H., and D. Martin, Adjoint sensitivity of episodic ozone in the Paris area to emissions on the continental scale, *J. Geophys. Res.*, *108*(D17), 8,561, 2003.

Simpson, D., et al., Inventorying emissions from nature in Europe, *J. Geophys. Res.*, *104*(D7), 8,113–8,152, 1999.

Stockwell, W. R., F. Kirchner, M. Kuhn, and S. Seefeld, A new mechanism for regional atmospheric chemistry modeling, *J. Geophys. Res.*, *102*(D22), 25,847–25,879, 1997.

Tao, Z., S. M. Larson, A. Williams, M. Caughey, and D. J. Wuebbles, Sensitivity of regional ozone concentrations to temporal distribution of emissions, *Atmos. Env.*, *38*(37), 6,279–6,285, 2004.

Troen, I., and L. Mahrt, A simple model of the atmospheric boundary layer; sensitivity to surface evaporation, *Boundary-Layer Meteorology*, *37*, 129–148, 1986.

Verwer, J. G., W. H. Hundsdorfer, and J. G. Blom, Numerical time integration for air pollution models, *Tech. rep.*, CWI, 1998.

Wesely, M. L., Parameterization of surface resistances to gaseous dry deposition in regional-scale numerical models, *Atmos. Env.*, *23*, 1,293–1,304, 1989.

Zhang, L., J. R. Brook, and R. Vet, A revised parameterization for gaseous dry deposition in air-quality models, *Atmos. Chem. Phys.*, *3*, 2,067–2,082, 2003.

Vivien.Mallet@cerea.enpc.fr, Bruno.Sportisse@cerea.enpc.fr